International Journal of Fracture **88:** 187–203, 1997.

Failure of a porous solid from a deep notch

P. REDANZ[1], N. A. FLECK[2] and R. M. McMEEKING*[2]
[1] *Department of Solid Mechanics,Technical University of Denmark, DK-2800 Lyngby, Denmark*
[2] *Cambridge University Engineering Department,Trumpington St, Cambridge CB2 1PZ, U.K.*

Received 30 May 1997; accepted in revised form 12 January 1998

Abstract. A finite strain finite element method is used to examine the stress state near the tip of a deep notch in an elastic-plastic porous solid. The notch is loaded in mode I plane strain tension and small scale yielding is assumed. Two rate independent strain hardening material models are used: a version of the Gurson model (1977) and the more recent FKM model developed by Fleck, Kuhn and McMeeking (1992). Under increasing K_{I}, void growth is initially stable and independent of mesh dimension. Localization of plastic flow sets in at a finite value K_i, and the deformation field is mesh-size dependent thereafter. The initiation of crack growth at the notch root is assumed to occur when a critical level of porosity is attained. The results show that the shape of the plastic zone for both the Gurson and the FKM material is highly dependent on the initial porosity. In the case of low initial porosity, the plastic zone shape is similar to that of a fully dense material; at higher initial porosities the plastic zone is concentrated ahead of the notch tip. The effect of the initial void volume fraction on the porosity field and the critical stress intensity factor is studied, and the mesh-size dependence of the results is discussed. The analysis is useful for prediction of the notched strength of porous metals.

1. Introduction

Sintered metals are used increasingly in the production of engineering components due to the advantages which they offer in terms of the ease of processing and mechanical properties. Complex shaped components such as gears and cams can be made to near net final shape from metallic powders. A characteristic feature of sintered materials is their porosity, which ranges from zero up to 0.5. The porosity may be used to advantage in gears and bearings by permitting the impregnation of the material with a liquid or solid lubricant. When the part contains a deep notch, failure may be by void growth from the notch root. Tensile stresses at the notch root lead to void growth and coalescence: a crack is nucleated. The main aim of the current paper is to develop a failure criterion for the nucleation of cracking from a notch root. The finite element method is used to examine the notch tip stress and deformation state in a porous solid.

The geometry of interest is shown in Figure 1. We consider a long notch of initial tip radius $\delta_0/2$ in a ductile porous solid. Mode I small scale yielding conditions are assumed, whereby the remote elastic field is characterised by the mode I stress intensity factor K_{I}. We shall show that under increasing K_{I} void growth is initially stable and independent of mesh dimension. Localization of plastic flow sets in at a finite value K_i, and the deformation field is mesh-size dependent thereafter. The criterion for the initiation of ductile crack growth is assumed to be the attainment of a critical void volume fraction, f_c. The results lead to the prediction of a critical stress intensity factor K_c as a function of initial porosity.

* On leave from Department of Mechanical Engineering, University of California, Santa Barbara, CA 93106, U.S.A.

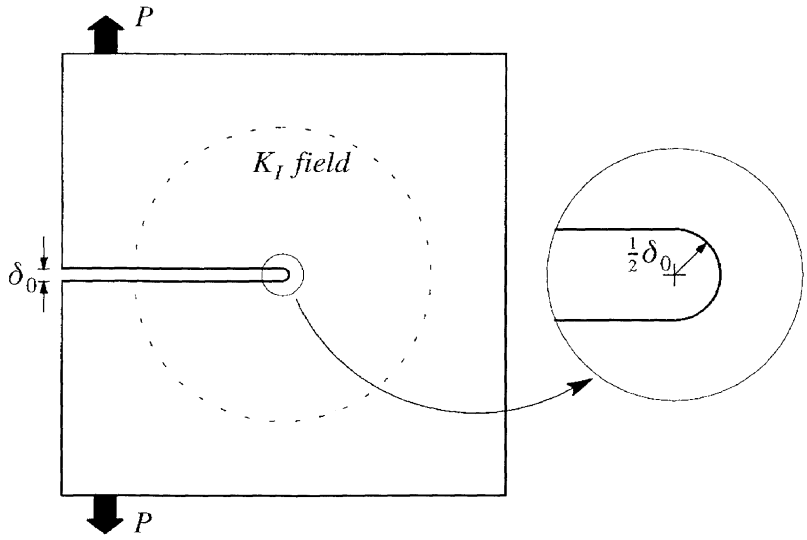

Figure 1. The small scale yielding problem for a long blunted notch in a porous solid. The area around the notch tip is shown enlarged to show the finite notch root radius $\frac{1}{2}\delta_0$.

In the present work two porous material models are studied: the Gurson model (1977) and the more recent FKM model developed by Fleck, Kuhn and McMeeking (1992). The Gurson material model, which is appropriate for low porosities, considers the porous material as a plastic matrix containing separated, spherical voids. In the limit of zero porosity, the Gurson model reduces to J_2-flow theory. The FKM model assumes that a porous material consists of spherical particles bonded perfectly at isolated contacts. The FKM model is applicable at higher porosities from about 0.10 up to the limit of dense random packing for equi-sized spheres; at dense random packing the void volume fraction f is 0.36.

The Gurson model has been used widely in the study of ductile fracture. For example, Drugan and Miao (1992, 1993, 1995) performed analytical analyses of the stress distribution around both a stationary and a growing crack tip for the case of a Gurson solid at fixed porosity. Other work on the effects of porosity on crack fields in ductile metals has consisted mainly of numerical studies, see for example Jagota et al. (1987); Aoki et al. (1984) and (1987); Needleman and Tvergaard (1987); and Aravas and McMeeking (1985), all using the Gurson model. Pan and co-workers (1990, 1991, 1994) have studied the crack tip stress fields and the plastic zones in pressure-sensitive materials using both asymptotic methods and the finite element method. They use a linear combination of the effective stress and the mean stress as the yield criterion; no porosity parameter is involved explicitly in their work in contrast to the treatment given below.

It is well-known that void growth leads to material softening and to the phenomenon of strain localization. The localization is associated with local unloading of material elements and to a switch of the governing field equations from elliptic to hyperbolic in nature. Post-localization, the response is sensitive to mesh size with a coarser mesh giving the stiffer response. In the current study, void growth is considered to well past localization and the role of mesh size is explored. We consider the geometry of a deep notch of initial opening δ_0 and root radius $\delta_0/2$ in order to set a length scale to the problem and to introduce a finite stress concentration at the notch root. Localization is expected to initiate at a finite value of K_I, independent of mesh size provided the mesh is sufficiently fine in relation to δ_0. Subsequently, deformation is localized within a band of thickness equal to the mesh size, and the post-

localization response is mesh-size dependent. In the limit of a vanishing root radius, the notch becomes a crack and the strain state at the crack tip is unbounded. Then, the smaller the mesh the lower is the critical value of K_I corresponding to the onset of localization.

2. Constitutive relations

The analysis is based on a convected co-ordinate Lagrangian formulation of the field equations, in which g_{ij} and G_{ij} are the metric tensors in the reference configuration and the current configuration, respectively, with determinants g and G. The Lagrangian strain tensor is $\eta_{ij} = \frac{1}{2}(G_{ij} - g_{ij}) = \frac{1}{2}(u_{i,j} + u_{j,i} + u^k_{,i} u_{k,j})$ where u^i are the displacement components on the reference base vectors, and $(\,)_{,i}$ denotes the covariant derivatives in the reference frame. The contravariant components of the Kirchhoff stress tensor, τ^{ij}, on the current base vectors are related to the contravariant components of the Cauchy or true stress tensor by $\tau^{ij} = \sqrt{G/g}\sigma^{ij}$. The initial state is taken as the reference configuration.

The strain increment is assumed to be the sum of the elastic and plastic parts, $\dot{\eta}_{ij} = \dot{\eta}^E_{ij} + \dot{\eta}^P_{ij}$, where $(\dot{})$ denotes differentiation with respect to a loading parameter. The elastic part of the strain is taken to be small and therefore the elastic constitutive response is approximately given by the hypoelastic relation

$$\overset{\nabla}{\sigma}{}^{ij} = \mathcal{R}^{ijkl}\dot{\eta}^E_{kl} = \mathcal{R}^{ijkl}(\dot{\eta}_{kl} - \dot{\eta}^P_{kl}), \tag{1}$$

where the Jaumann (co-rotational) rate of the Cauchy stress tensor, $\overset{\nabla}{\sigma}{}^{ij}$, is related to the convected rate by

$$\overset{\nabla}{\sigma}{}^{ij} = \dot{\sigma}^{kl} + \tfrac{1}{2}\{G^{ik}\sigma^{jl} + G^{jk}\sigma^{il} + G^{il}\sigma^{jk} + G^{jl}\sigma^{ik}\}\dot{\eta}_{kl}. \tag{2}$$

The finite strain generalization of Budiansky (see Hutchinson, (1973)) is used

$$\mathcal{R}^{ijkl} = \frac{E}{1+\nu}\left\{\tfrac{1}{2}\left(G^{ik}G^{jl} + G^{il}G^{jk}\right) + \frac{\nu}{1-2\nu}G^{ij}G^{kl}\right\}, \tag{3}$$

where E and ν are Young's modulus and Poisson's ratio, respectively. Equilibrium is enforced via the principle of virtual work

$$\int_V \tau^{ij}\delta\eta_{ij}\,\mathrm{d}V = \int_S T^i\delta u_i\,\mathrm{d}S, \tag{4}$$

with body forces neglected. Here V and S are the volume and the surface of the body in the reference state. The components of the surface tractions per unit area in the reference configuration on the reference base vectors are given by

$$T^i = (\tau^{ij} + \tau^{kj}u^i_{,k})n_j, \tag{5}$$

with n_j as the components of the surface normal in the reference state.

For time independent plasticity the resulting incremental constitutive relations are of the form

$$\dot{\tau}^{ij} = L^{ijkl}\dot{\eta}_{kl}. \tag{6}$$

The uniaxial true stress-logarithmic strain curve for the matrix material in tension is represented by the piecewise power law

$$\epsilon = \begin{cases} \sigma/E & \sigma \leqslant \sigma_y \\ \dfrac{\sigma_y}{E}\left(\dfrac{\sigma}{\sigma_y}\right)^n & \sigma > \sigma_y, \end{cases} \tag{7}$$

where σ_y is the uniaxial yield stress and n is the strain hardening exponent.

3. Porous material models

The yield surface for a porous material depends upon the stress state σ^{ij}, the yield strength of the matrix σ_M and the void volume fraction f; the yield function Φ can be written in the form

$$\Phi(\sigma^{ij}, \sigma_M, f) = 0. \tag{8}$$

3.1. GURSON MODEL

The Gurson model (1977) assumes that porosity exists in the form of isolated, spherical voids. The model has a sound micromechanical basis, and gives accurate estimates of the macroscopic softening due to a small volume fraction of voids including the dilute limit. Much use has been made of the Gurson model to investigate void growth in the context of ductile fracture of notched bars (see for example, Becker et al. (1988) and Needleman and Tvergaard (1984)) and at crack tips (Needleman and Tvergaard (1987) and (1994)). The applicability of the Gurson solid to sintered materials has been examined by Hancock (1982) and Becker (1987) amongst others and is reviewed by Tvergaard (1990). Although measurements of the yield surface shape at low porosities appear to be missing from the literature, the Gurson solid appears to give a satisfactory prediction of uniaxial compression data (e.g. Hancock (1982)) and of notched tensile data (Becker et al. (1988)). The model loses accuracy at porosities in excess of about $f = 0.1$. In this study, an elastic-strain hardening plastic version of the model is used. The yield surface is given by

$$\Phi = \frac{\sigma_e^2}{\sigma_M^2} + 2q_1 f \cosh\left\{\frac{q_2}{2}\frac{\sigma_k^k}{\sigma_M}\right\} - \left(1 + (q_1 f)^2\right) = 0, \tag{9}$$

with the macroscopic effective Mises stress given by $\sigma_e = (3s_{ij}s^{ij}/2)^{1/2}$ in which $s^{ij} = \sigma^{ij} - G^{ij}\sigma_k^k/3$ is the stress deviator. The constants q_1 and q_2 are the Tvergaard adjustment factors (1981, 1982a) set to 1.5 and 1.0, respectively, in the present study. In the limit of zero porosity the Gurson model reduces to J_2-flow theory.

3.2. FKM MODEL

The more recent FKM porous material model suggested by Fleck, Kuhn and McMeeking (1992) assumes that the material consists of spherical particles joined by discrete necks. The FKM solid is based on an upper bound calculation for the yield surface of a particulate solid; it assumes that the imposed macroscopic strain rate defines the normal indentation rate and the associated plastic dissipation at isolated contacts between particles. The FKM model is

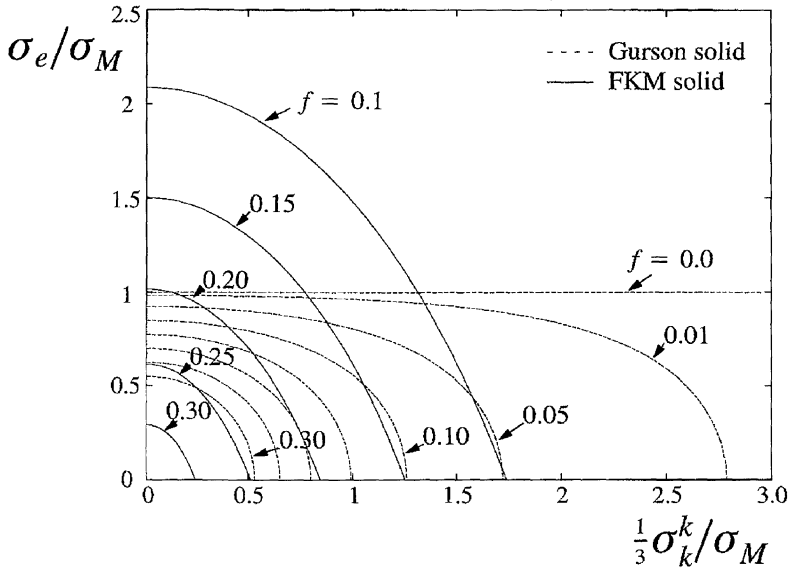

Figure 2. Comparison of the yield surfaces for the Gurson model and the FKM model.

applicable at higher porosities from approximately 0.10 up to the limit of dense random packing, taken to be that for equi-sized spheres, $f = \hat{f} = 0.36$ (This corresponds to a relative density $D = 0.64$). The yield surface is given by

$$\Phi = \left(\frac{5}{18}\frac{\sigma_e}{p_y} + \frac{2}{3}\right)^2 + \left(\frac{\sqrt{5}}{3}\frac{\frac{1}{3}\sigma_k^k}{p_y}\right)^2 - 1 = 0, \tag{10}$$

with

$$p_y = 2.97(1-f)^2\frac{\hat{f}-f}{\hat{f}}\sigma_M. \tag{11}$$

Figure 2 shows a comparison of the FKM yield surface and that of the Gurson model. The FKM yield surface contains a vertex on the hydrostatic stress axis in $(\sigma_e, \frac{1}{3}\sigma_k^k)$ space. For numerical computation purposes, the vertex is rounded off by a quadratic approximation to the yield surface near the vertex as done by Fleck, Otoyo and Needleman (1992).

The Gurson model is appropriate at low levels of porosity $f < 0.1$ when voids are rounded and discrete. In contrast, the FKM model attempts to capture the macroscopic response at high porosity $f > 0.1$ for the case of isolated deformation at the necks between particles. It is clear from Figure 2 that the shape and size of the yield surfaces are markedly different for the two models: the FKM model has a higher ratio of deviatoric strength to hydrostatic strength, for all porosity levels less than about $f = 0.3$. Both models display approximately the same rate of softening of hydrostatic strength with increasing f; the FKM model, however, predicts that the deviatoric strength decreases more rapidly with increasing f than the Gurson solid. At porosity levels of about $f = 0.1$, it might be hoped that the yield surfaces for the two models would converge. Unfortunately, this is not the case, due to the different micromechanical basis for the two models. In reality, for f in the vicinity of 0.1, the microstructure of sintered solids consists of interconnected voids, and yielding occurs throughout the particles rather than in a local manner at individual necks: both models are only approximately realistic in

this difficult transition regime. Fleck et al. (1992) suggest that in this transition regime it is more appropriate to take a weighted average of the FKM yield surface and the Gurson yield surface than to assume that either model is realistic.

Few experimental data are available to reveal the true shape of the yield surface as a function of porosity. In recent powder compaction experiments by Akisanya et al. (1997), the yield surface of isostatically compacted copper powder was measured for porosities in the range $f = 0.1 - 0.2$. Good agreement was observed between the prediction of yield surface shape by a cohesionless version of the FKM model (Fleck (1995)) and the observed yield surface. No comparison was made between the predicted size of the yield surface by the FKM model and the measured yield surface, as the yield strength of the copper powder was not known. As discussed in the original paper by Fleck et al. (1992), the size of the FKM yield surface is not realistic at porosity levels of less than $f = 0.2$, as it erroneously predicts that the macroscopic von Mises flow strength σ_e exceeds the yield strength σ_M of the base powder material. This is traced back to the fact that the model assumes that the normal traction at inter-particle contacts is given by the Prandtl indentation solution of three times. Recent calculations of the contact pressure between powder particles by Ogbonna and Fleck (1995) and by Mesarovic and Fleck (1998) reveal that the degree of plastic constraint at the necks between particles is significantly less than the Prandtl value for porosities in the range $f = 0.1 - 0.2$. We conclude that the shape of the FKM yield surface has experimental support for f greater than about 0.1, but the size of the yield surface is somewhat overestimated.

3.3. Basic porous material equations

A detailed discussion of the procedure for the Gurson material is given by Tvergaard (1990); here, only a brief summary is reported. Since the elastic deformations are small compared to the plastic deformations the elastic contribution to the change in f with deformation is neglected. The matrix material is plastically incompressible, and so the rate of growth of the porosity is given by

$$\dot{f} = (1 - f)G^{ij}\dot{\eta}^P_{ij}. \tag{12}$$

The incremental relation between the effective plastic strain in the matrix, ϵ^P_M, and the equivalent tensile yield strength of the matrix, σ_M, is given by

$$\dot{\epsilon}^P_M = \left(\frac{1}{E_t} - \frac{1}{E}\right)\dot{\sigma}_M, \tag{13}$$

where E_t is the slope of the uniaxial true stress-logarithmic strain curve for the matrix material. Here, σ_M and ϵ^P_M are viewed as spatial averages of the actual microscopic fields in the matrix material.

The plastic part of the strain increment is assumed to be

$$\dot{\eta}^P_{ij} = \Lambda\frac{\partial\Phi}{\partial\sigma^{ij}}, \tag{14}$$

where Λ is the plastic multiplier and $\partial\Phi/\partial\sigma^{ij}$ gives the direction of the plastic strain increment. Normality for the matrix material at the microscopic level implies macroscopic

normality for the porous aggregate (Berg, 1970; Bishop and Hill, 1951). The macroscopic plastic work rate is equated with the plastic work rate in the matrix material, giving

$$\sigma^{ij}\dot{\eta}^P_{ij} = F(f)\sigma_M\dot{\epsilon}^P_M, \tag{15}$$

where $F(f)$ is the volume fraction of deforming material. In the Gurson model $F(f) = 1-f$ since all of the matrix material in the original model is assumed to yield. An expression for F(f) in the FKM model is taken from Fleck, Otoyo and Needleman (1992) as

$$F = \frac{45}{\sqrt{3}}(1-f)^2\left(\frac{\hat{f}-f}{\hat{f}}\right)^{3/2}. \tag{16}$$

Using (13) and (15), the rate of the tensile equivalent flow stress in the matrix material follows as

$$\dot{\sigma}_M = \frac{EE_t}{E-E_t}\frac{\sigma^{ij}\dot{\eta}^P_{ij}}{F(f)\sigma_M}. \tag{17}$$

Initiation of plastic yielding occurs when $\Phi = 0$ and $\dot{\Phi} > 0$. The consistency condition for continued plastic flow, $\dot{\Phi} = 0$, is used to obtain an expression for the plastic multiplier Λ, and thereby the plastic strain increment,

$$\dot{\eta}^P_{ij} = \frac{1}{H}\frac{\partial\Phi}{\partial\sigma^{ij}}\frac{\partial\Phi}{\partial\sigma^{kl}}\overset{\nabla}{\sigma}{}^{kl}, \tag{18}$$

with

$$H = -\left(\frac{\partial\Phi}{\partial f}(1-f)G^{ij} + \frac{\partial\Phi}{\partial\sigma_M}\frac{EE_t}{E-E_t}\frac{\sigma^{ij}}{F(f)\sigma_M}\right)\frac{\partial\Phi}{\partial\sigma^{ij}}. \tag{19}$$

Upon substituting (18) into (1), the instantaneous moduli from (6) are determined as

$$L^{ijkl} = \mathcal{L}^{ijkl} - \mu M^{ij}M^{kl}, \tag{20}$$

where

$$\mathcal{L}^{ijkl} = \sqrt{\frac{G}{g}}\left\{\mathcal{R}^{ijkl} - \tfrac{1}{2}(\sigma^{ik}G^{jl} + \sigma^{jk}G^{il} + \sigma^{il}G^{jk} + \sigma^{jl}G^{ik}) + \sigma^{ij}G^{kl}\right\} \tag{21}$$

$$\mu = \begin{cases} 0 & \text{elastic unloading} \\ \sqrt{\dfrac{G}{g}}\left[H + \dfrac{\partial\Phi}{\partial\sigma^{rs}}\mathcal{R}^{rskl}\dfrac{\partial\Phi}{\partial\sigma^{kl}}\right]^{-1} & \text{plastic loading} \end{cases} \tag{22}$$

and M^{ij} is defined by

$$M^{ij} = \mathcal{R}^{ijkl}\frac{\partial\Phi}{\partial\sigma^{kl}}. \tag{23}$$

4. Numerical method

The finite element mesh used for the calculations is shown in Figure 3a. The mesh consists of 1718 nodes and 524 isoparametric eight-noded elements. An enlargement of the near tip region is shown in Figure 3b. Due to symmetry about the crack line, only half of the body is analysed, as shown. The calculations for the porous material are carried out with 3x3 Gauss integration points in each element. The ratio between the initial notch opening, δ_0, and the outer mesh radius, R_b, is 1/2500.

The reference state is represented by a Cartesian coordinate system x^1-x^2 and a state of plane-strain deformation is assumed. The origin of the Cartesian frame is set at the center of the semi-circular notch tip in Figure 3b. Numerical solutions are obtained by an incrementally linear method. An approximate equilibrium state is fulfilled for the current values of the stresses, σ^{ij}, the strains, η_{ij}, etc. By expanding the principle of virtual work (4) about this known state, the equations regarding the increments, $\dot{\sigma}^{ij}$, $\dot{\eta}_{ij}$, etc. are obtained. With body forces neglected, the expansion of the principle of virtual work takes the form

$$\int_V \left\{\dot{\tau}^{ij}\delta\eta_{ij} + \tau^{ij}\dot{u}^k_{,i}\delta u_{k,j}\right\} \mathrm{d}V$$

$$= \int_S \dot{T}^i \delta u_i \,\mathrm{d}S - \left[\int_V \tau^{ij}\delta\eta_{ij}\,\mathrm{d}V - \int_S T^i \delta u_i \,\mathrm{d}S\right]. \tag{24}$$

The term in square brackets of (24) vanishes according to (4), if the current state satisfies equilibrium. It is included here to prevent the solution from drifting away from the true equilibrium state.

The value of the parameter μ in (20) is chosen at each material point according to the state of the material in the previous increment. This type of procedure gives good accuracy provided the increments are sufficiently small (see for example Tvergaard (1982b)).

Small-scale yielding conditions are assumed and the remote field is the mode I K-field. The displacement boundary conditions imposed at the outer semi-circular boundary are of the form

$$\begin{Bmatrix} u_1 \\ u_2 \end{Bmatrix} = \frac{K_\mathrm{I}}{E}(1+\nu)\sqrt{\frac{R_b}{2\pi}} \begin{Bmatrix} \left(1 - 2\nu + \sin^2\tfrac{1}{2}\theta\right)\cos\tfrac{1}{2}\theta \\ \left(2 - 2\nu + \cos^2\tfrac{1}{2}\theta\right)\sin\tfrac{1}{2}\theta \end{Bmatrix}, \tag{25}$$

where u_1 and u_2 are the Cartesian components of the displacement vector and (r, θ) are polar co-ordinates as defined in Figure 3. K_I is the mode I stress intensity factor. The remaining boundary conditions are

$$\begin{aligned} &T^i = 0 \text{ on the crack surface} \\ &T^1 = 0, u_2 = 0 \text{ for } x^2 = 0, x^1 \geqslant \tfrac{1}{2}\delta_0 \end{aligned} \tag{26}$$

5. Results

In a typical finite element calculation, the notched porous solid is loaded with an increasing K_I, and the evolution of stress state and porosity is determined. Initially, at small values of K_I,

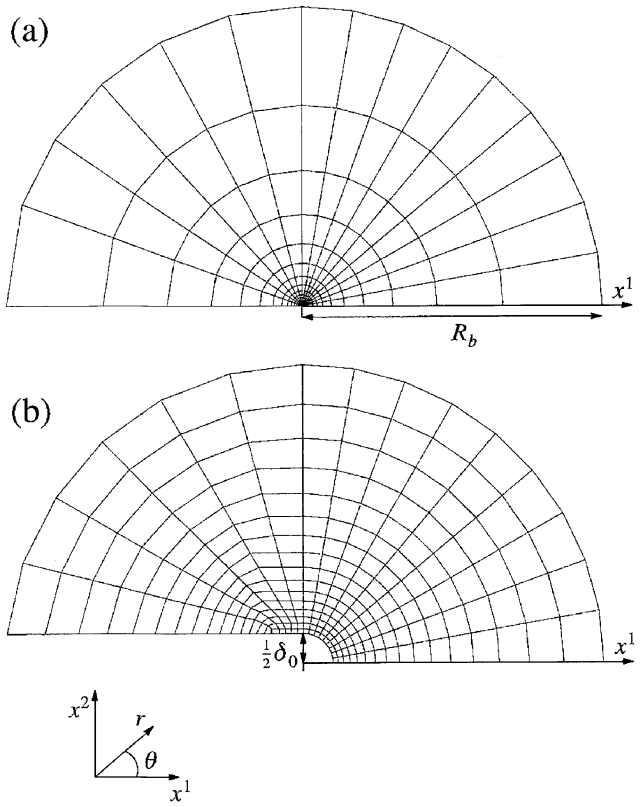

Figure 3. Finite element mesh in initial configuration (medium mesh, $l_0/\delta_0 = 0.087$): (a) full mesh, and (b) enlarged near tip region of mesh.

plastic deformation and attendant void growth occur in a stable manner in the vicinity of the notch root. In this regime the response is independent of mesh size for a sufficiently refined mesh in relation to the notch opening δ_0. At a particular value of K_I, termed K_i, localization of deformation with elastic unloading initiates at some point in the mesh. Thereafter, material loads within a narrow band near the notch root and adjacent material unloads. The width of the band of continuing localized deformation is set by the mesh size, and the post-localization reponse is thereby mesh-size dependent. The initiation of ductile crack growth, which may eventually lead to failure, is defined to occur when the porosity attains a critical value, $f_{\max} = f_c$ at any material point. This condition defines the critical stress intensity factor, K_c, at which fracture begins by void coalescence. We shall show that the critical void volume fraction f_c is attained only in the post-localisation regime and that the particular choice of value for f_c has a negligible effect on the calculated value of K_c. Void growth is rapid in the post-localisation regime, and the precise details depend as much upon the degree of mesh refinement as upon the assumed softening law. The reader is referred to Tvergaard and Needleman (1984) for a suggested modification to the Gurson model such that the strength of the solid reduces to zero when a critical porosity is attained.

Both the Gurson model and the FKM model predict softening responses which lead to mesh size dependence in the post-localization regime. Needleman and Tvergaard (1994) have discussed these mesh effects for the Gurson model. Here, calculations are carried out for three different meshes, $l_0/\delta_0 = 0.131$, $l_0/\delta_0 = 0.087$ and $l_0/\delta_0 = 0.052$, where l_0 is the initial height of the first element directly ahead of the notch tip. The median mesh, $l_0/\delta_0 = 0.087$, is the one shown in Figure 3 and is used in all calculations unless otherwise stated. The calculations are

carried out for a matrix material with $\sigma_y/E = 0.0025$, $\nu = 0.3$ and strain hardening exponent,. $n = 10$.

The maximum porosity at any point within the mesh is plotted as a function of stress intensity factor, K_I, for the three different meshes. Results are given in Figure 4a for the Gurson solid (for an initial porosity $f_0 = 0.05$) and in Figure 5a for the FKM solid (for an initial porosity $f_0 = 0.14$). For both material models the R-curves are insensitive to mesh size prior to localization, but become strongly sensitive to mesh size in the post-localization regime. After localization, void growth occurs more easily in the fine mesh and the estimated fracture toughness value, K_c, corresponding to $f_{max} = f_c = 0.20$, decreases with decreasing mesh size, as shown in Figures 4a and 5a. In the limit of vanishing mesh size we would expect $K_c = K_i$. Thus, the value K_i serves as a useful measure of the notch toughness.

For low initial porosities such as $f_0 = 0.05$, the Gurson solid is the appropriate constitutive model and stable plastic void growth occurs for a large range of K_I; localization sets in when the void volume fraction has approximately doubled from its initial value. At higher initial porosities, such as $f_0 = 0.14$, the FKM solid is appropriate; localization occurs at a low level of K_I and the void volume fraction has increased by about 10 percent above its initial value.

Typical plots of the plastic zone shape are shown in Figure 4b for the Gurson solid, and in Figure 5b for the FKM solid. X_0 is the horizontal distance from the center of the semi-circular notch tip to a point of interest, such as the plastic zone boundary. It is again evident that, prior to localization, there is a negligible effect of mesh size on the response. This is illustrated for the Gurson solid in Figure 4b: the plastic zone boundary is shown for $K_c/\sigma_y\sqrt{\delta_0} = 11$, labelled state C for the coarse mesh and state D for the fine mesh. The plastic zone shape is reminiscent of that for a plane strain mode I crack in a von Mises solid. A similar insensitivity of results to mesh size prior to localization is observed for the FKM solid, see Figure 5b. Therein, the plastic zone boundary is shown for $K_c/\sigma_y\sqrt{\delta_0} = 1.4$, labelled state C for the coarse mesh and state D for the fine mesh. For the FKM solid the plastic zone is concentrated ahead of the notch tip; this is suggestive of a plane stress Dugdale model of notch root plasticity. The difference in shapes of plastic zone for the two material models is consistent with the difference in shape of the yield surfaces. The FKM solid has a much lower ratio of hydrostatic yield strength to deviatoric yield strength compared with the Gurson solid, and high stress triaxiality is unable to develop ahead of the notch. Consequently, the plastic zone shape is similar to that generated in a fully dense solid under plane stress conditions. In contrast, the Gurson solid can support larger hydrostatic stresses and the plastic zone shape is similar to that at the tip of a mode I crack under plane strain conditions.

The plastic zone shapes at the onset of fracture (e.g. $f_{max} = f_c = 0.20$) are included in Figures 4b and 5b. The critical state is labelled A for the coarse mesh ($l_0/\delta_0 = 0.131$), and labelled B for the fine mesh ($l_0/\delta_0 = 0.052$), as cross-referenced on the R-curves of Figures 4a and 5a. For both constitutive descriptions, a larger value of K_c and a larger plastic zone size are exhibited by the coarser mesh. The localized strip of plastically deforming material directly ahead of the notch tip has the height of 2 integration points and extends a couple of notch openings ahead of the notch.

The notch opening displacements are $\delta/\delta_0 = 1.244$ and $\delta/\delta_0 = 1.178$ at points B and D in Figure 4a, respectively, for the Gurson material with low initial porosity. When the FKM model with high initial porosity is used the notch opening displacement is $\delta/\delta_0 = 1.017$ in state B and $\delta/\delta_0 = 1.008$ in state D in Figure 5a.

The tensile stress component $\hat{\sigma}_{22}$ is plotted as a function of distance directly ahead of the notch for states B and D in Figure 4c (Gurson solid), and in Figure 5c (FKM solid). Prior to

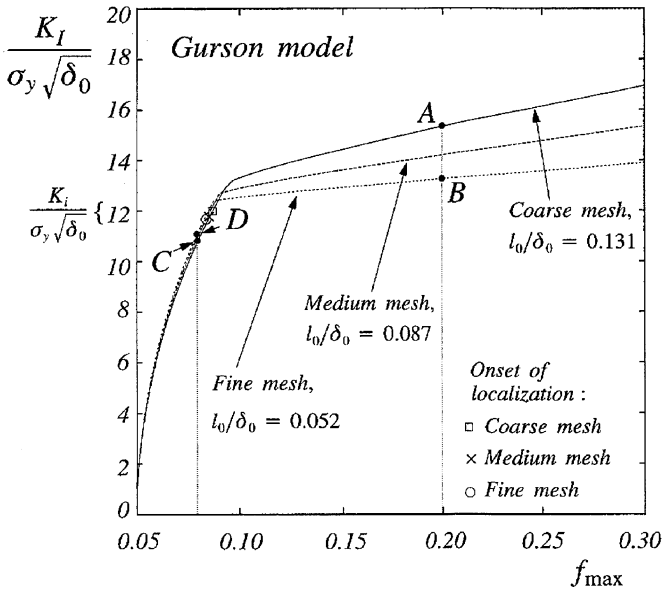

(a)

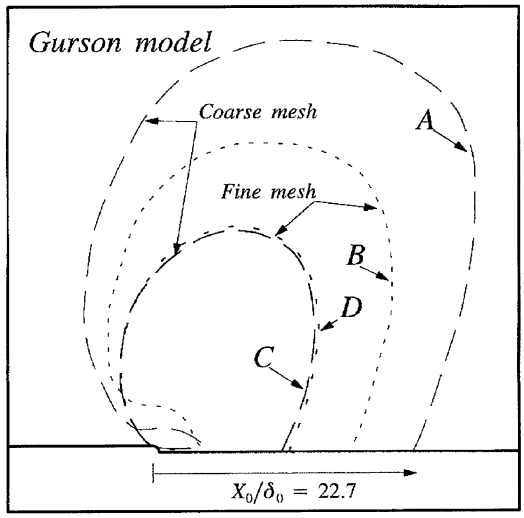

(b)

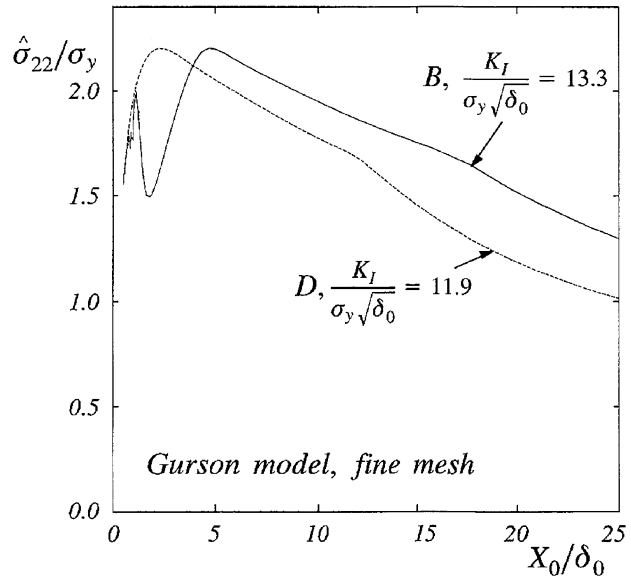

(c)

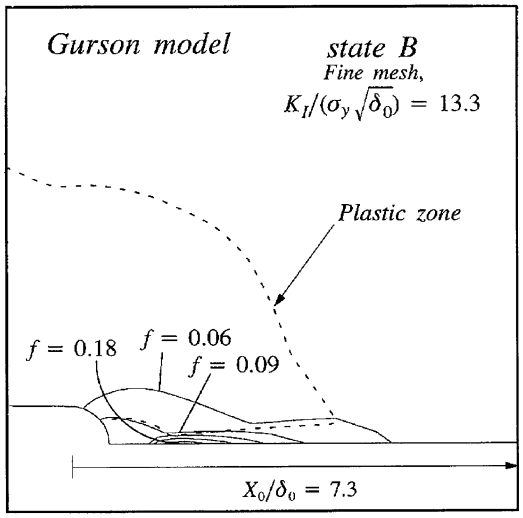

(d)

Figure 4. Results for the Gurson model with the initial porosity $f_0 = 0.05$. (a) The stress intensity factor, K_I, as a function of the maximum porosity for three different meshes, $l_0/\delta_0 = 0.131$, $l_0/\delta_0 = 0.0.087$ and $l_0/\delta_0 = 0.052$. The onset of localization is marked for each mesh. (b) The plastic zone boundary at $f_{max} = 0.2$ for the coarse mesh (state A) and for the fine mesh (state B) post-localization, and at $f_{max} = 0.08$ for the coarse mesh (state C) and for the fine mesh (state D) pre-localization. (c) The tensile stress directly ahead of the notch $\hat{\sigma}_{22}$ normalised by the yield stress σ_y, as a function of the initial horizontal distance from the center of the semi-circular notch tip X_0, for states B and D. (d) The plastic zone and porosity contours for state B.

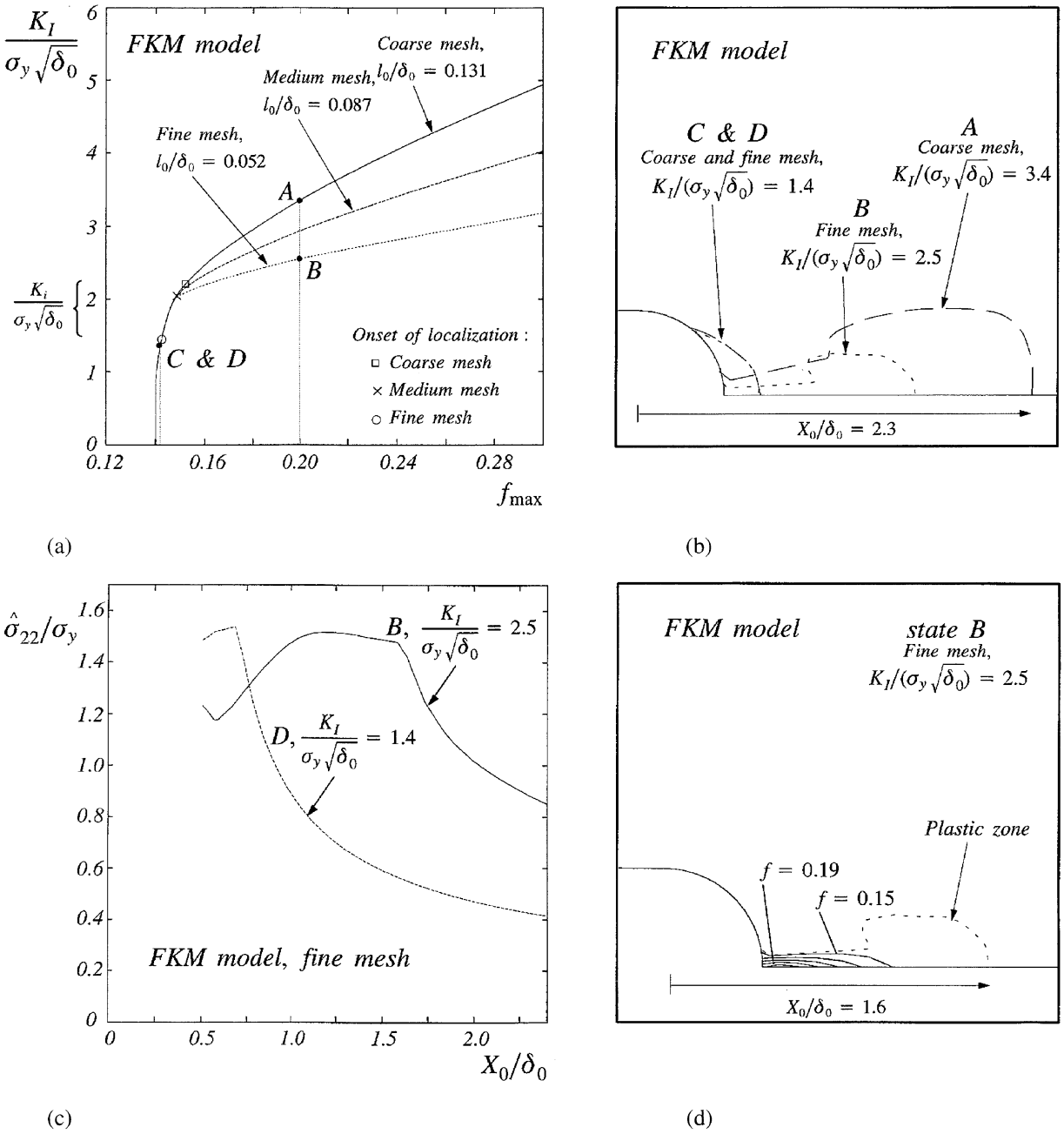

Figure 5. Results for the FKM model with the initial porosity $f_0 = 0.14$. (a) The stress intensity factor, K_I, as a function of the maximum porosity for three different meshes, $l_0/\delta_0 = 0.131$, $l_0/\delta_0 = 0.0.087$ and $l_0/\delta_0 = 0.052$. The onset of localization is marked for each mesh. (b) The plastic zone boundary at $f_{max} = 0.2$ for the coarse mesh (state A) and for the fine mesh (state B) post-localization, and at $f_{max} = 0.142$ for the coarse mesh (state C) and for the fine mesh (state D) pre-localization. (c) The tensile stress directly ahead of the notch $\hat{\sigma}_{22}$ normalised by the yield stress σ_y, as a function of the initial horizontal distance from the center of the semi-circular notch tip X_0, for states B and D. (d) The plastic zone and porosity contours for state B.

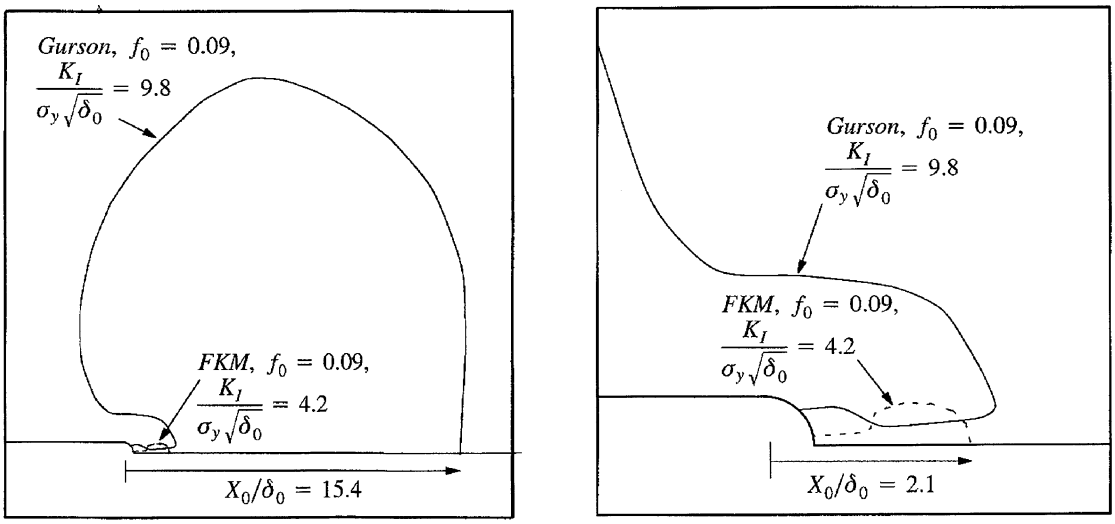

Figure 6. Comparison of the plastic zones from the FKM model and the Gurson model with the same initial porosity, $f_0 = 0.09$, and the same critical porosity, $f_c = 0.20$. (a) full size of both plastic zones, and (b) an enlargement of the near tip region.

localization (state B) the stress distribution $\hat{\sigma}_{22}$ is similar to that for a blunted crack in a strain hardening fully dense solid (Rice and Johnson (1970), and McMeeking (1977)). The stress attains a peak value at a distance ahead of the notch of approximately the notch root radius. At the later stages of loading, when $f_{\max} = 0.20$ at state B, the stress peak has moved away from the notch tip. Between the notch tip and the location of the stress peak plastic deformation has localized and the stress level has decreased due to void growth. The unstable nature of the void growth within the band is clear from the highly localized contours of porosity as shown for the fine mesh at $f_{\max} = f_c = 0.20$ in Figures 4d and 5d. The highly local void growth at the notch root is consistent with the predictions of Aravas and McMeeking (1985), who examined the rupture of the ligament between a blunt crack and a neighbouring void. In reality an additional material length scale is involved, in the form of the finite spacing of void-nucleating particles, such as carbide particles in steels. In order to model this feature an additional length scale is required within the constitutive description, for example by the addition of a cohesive zone ahead of the notch tip, as implemented by Tvergaard and Hutchinson (1992), or by use of a non-local plasticity law, see for example Fleck and Hutchinson (1997).

A comparison of the plastic zones for the two material models is given in Figure 6. In both cases, the initial porosity is $f_0 = 0.09$ and the critical porosity, $f_c = 0.20$ has been attained. The medium mesh ($l_0/\delta_0 = 0.087$) is used. The plastic zone of the FKM model is concentrated near the notch tip and the critical stress intensity factor is much lower than in the Gurson material case. When the critical porosity is attained, the Gurson model predicts a critical stress intensity factor of $K_c/\sigma_y\sqrt{\delta_0} = 9.78$ which is approximately twice that of the FKM model ($K_c/\sigma_y\sqrt{\delta_0} = 4.20$). The size of the plastic zone of the Gurson model is also much larger than that of the FKM model. These differences may be explained in broad terms as follows. For a void volume fraction in the range 0.1 to 0.2, the FKM solid has a much lower ratio of hydrostatic strength to deviatoric strength than that of the Gurson solid. Also, the FKM solid softens more rapidly with increasing porosity. Consequently, the FKM solid

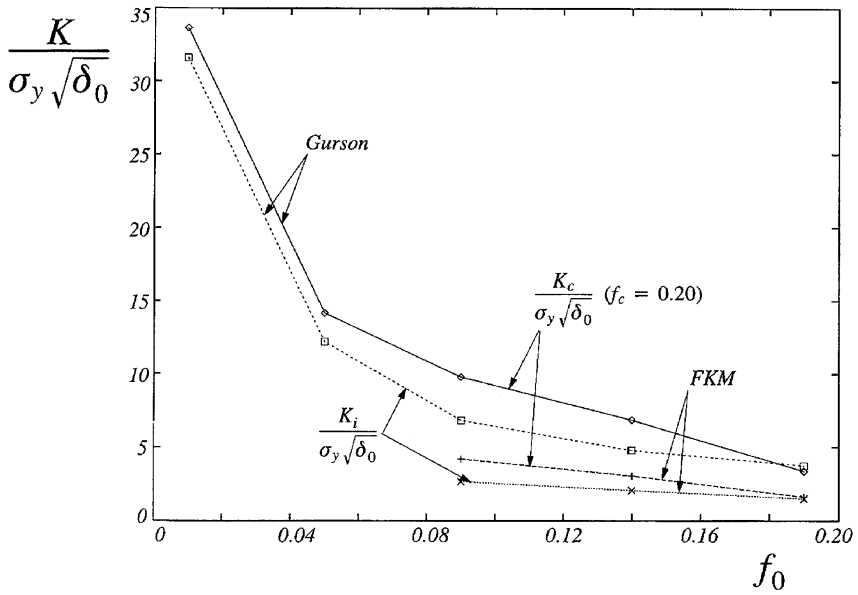

Figure 7. The normalized stress intensity factor for the initiation of localization K_i and the critical stress intensity factor K_c ($f_c = 0.20$) as functions of initial porosity, f_0.

is unable to support significant hydrostatic stresses and the usual plane strain plastic zone is unable to develop.

The stress intensity factor for the initiation of localization K_i and the critical stress intensity factor K_c for the initiation of ductile crack growth are both highly dependent on the initial porosity as shown in Figure 7. On the other hand, the assumed value of critical porosity has lesser effect on the magnitude of K_c: numerical experimentation revealed that an increase in f_c from 0.2 to 0.3 resulted in an increase of K_c by a few percent. We emphasize that predictions of K_i are not strongly dependent of the mesh but predictions of K_c are sensitive to the ratio of mesh size to initial notch opening. The results shown in Figure 7 pertain to $l_0/\delta_0 = 0.087$. As mentioned above, the Gurson model is the more realistic model at low porosities and the FKM model is more appropriate at higher porosities. The lowest initial porosity used with the FKM model is 0.09. At initial porosities higher than 0.10 the values of K_i and K_c for the Gurson model lie approximately a factor of two above those for the FKM model.

6. Discussion

It is clear that the deformation response becomes mesh size dependent at the onset of localization. It is suggested that the stress intensity factor K_i at localization is a useful measure of notch toughness, since it is slightly conservative, $K_i < K_c$, and is not strongly mesh dependent.

So far, the mesh size has been considered to be a modelling artifact with no physical significance. An alternative strategy is to assume that the mesh size is an approximate measure of the particle size of a sintered solid, and that material response depends upon this internal material length scale. Results for different mesh sizes are then ascribed a physical significance: results for a large mesh are representative of the behaviour of a sintered solid containing large particles, and results for a fine mesh apply to a sintered solid containing fine particles. The

fracture toughness of a sintered solid containing a sharp crack would then scale with the particle size.

With the chosen critical porosity criterion for initiation of ductile crack growth, the Gurson and FKM constitutive laws predict quite different plastic zones and critical stress intensity factors. The plastic zones predicted by the Gurson model are much larger than those predicted by the FKM model partly due to the larger value of the stress intensity factor when the critical porosity is attained. The FKM solid is unable to support large hydrostatic stresses and thus, the usual plane strain plastic zone is unable to develop. However, the material models are based on different assumptions and are valid for different ranges of porosity. The FKM model is thought to be valid for porosity f in the range 0.1 to 0.35, and the Gurson model is realistic for $f < 0.1$.

Despite the obvious difference between the material models, it has been shown that the shape and size of the plastic zone in general is highly dependent on the initial porosity of the material. In the case of low initial porosity, the shape of the plastic zone is quite similar to that of a crack tip field in a fully dense material except directly adjacent to the notch tip where the increase in porosity causes stress relaxation. At higher initial porosities, the plastic zone is small and concentrated ahead of the notch tip.

The maximum porosity in the present study is always located directly ahead of the notch tip. For the case of the Gurson solid with low initial porosity, only a small increase in porosity occurs as K is increased from zero to K_i. Specifically, the growth in porosity exceeds 1 percent only in a small region around the notch tip within a much large plastic zone. In contrast, for the FKM solid with high initial porosity, the region over which porosity grows by more than 1 percent as K is increased from zero to K_i occupies about half of the plastic zone.

The focus of the current work has been to use the onset of localisation as the failure criterion for a deep notch. Once localisation has set in, subsequent void growth is rapid. Although the post-localisation response is sensitive to the choice of constitutive model, to the mesh details and to the numerical method employed, the precise post-localisation response is of minor importance. There is little elevation in stress intensity beyond the point of localisation as evidenced by the fact that the critical stress intensity factor is close in value to the stress intensity factor at the onset of localisation. The magnitude of K_c is primarily dependent upon the initial porosity and is less dependent upon the choice of critical porosity.

Acknowledgements

The contribution of Pia Redanz's Ph.D. thesis advisor, Professor Viggo Tvergaard, is gratefully acknowledged. The work of Pia Redanz was financially supported by the MUP2 research programme Materials Processing, Properties and Modelling, financed by the Danish Agency for Development of Trade and Industry, the Danish Natural Science Research Council, and the Danish Technical Research Council. R.M. McMeeking was supported by a Visiting Professorship at Cambridge University, and is grateful for the financial support of the Cambridge Centre for Micromechanics.

References

Akisanya, A.R., Cocks, A.C.F. and Fleck, N.A. (1997). The yield behaviour of metal powders. *International Journal of Mechanical Science* **39**(12), 1315–1325.

Aoki, S., Kishimoto, K., Takeya, A. and Sakata, M. (1984). Effects of microvoids on crack blunting and initiation in ductile materials. *International Journal of Fracture* **24**, 267–278.

Aoki, S., Kishimoto, K., Yoshida, T. and Sakata, M. (1987). A finite element study of the near crack tip deformation of a ductile material under mixed mode loading. *Journal of the Mechanics and Physics of Solids* **35**(4), 431–455.

Aravas, N. and McMeeking, R.M. (1985). Microvoid growth and failure in the ligament between a hole and a blunt crack. *International Journal of Fracture* **29**, 21–38.

Becker, R. (1987). The effect of porosity distribution on ductile failure. *Journal of the Mechanics and Physics of Solids* **35**, 577–599.

Becker, R., Needleman, A., Richmond, O. and Tvergaard, V. (1988). Void growth and failure in notched bars. *Journal of the Mechanics and Physics of Solids* **36**, 317–351.

Berg, C.A. (1970). Plastic dilatation and void interaction. *Inelastic Behavior of Solids* (Edited by M.F. Kanninen, W.F. Adler, A.R. Rosenfield and R.I. Jaffee), McGraw-Hill, New York, 171–210.

Bishop, J.F.W. and Hill, R. (1951). A theory of the plastic distortion of a polycrystalline aggregate under combined stresses. *Philosophical Magazine* **42**, 414–427.

Dong, P. and Pan, J. (1991). Elastic-plastic analysis of cracks in pressure-sensitive materials. *International Journal of Solids Structures* **28**(9), 1113–1127.

Drugan, W.J. and Miao, Y. (1992). Influence of porosity on plane strain tensile crack-tip stress fields in elastic-plastic materials: Part I. *Journal of Applied Mechanics* **59**, 559–567.

Fleck, N.A. (1995). On the cold compaction of powders. *Journal of the Mechanics and Physics of Solids* **43**, 1409–1431.

Fleck, N.A. and Hutchinson, J.W. (1997). Strain gradient plasticity. *Advances in Applied Mechanics* **33**, 295–361.

Fleck, N.A., Otoyo, H. and Needleman, A. (1992). Indentation of porous solids. *International Journal of Solids and Structures* **29**(13), 1613–1636.

Fleck, N.A., Kuhn, L.T. and McMeeking, R.M. (1992). Yielding of metal powder bonded by isolated contacts. *Journal of the Mechanics and Physics of Solids* **40**(5), 1139–1162.

Gurson, A.L. (1977). Continuum theory of ductile rupture by void nucleation and growth: Part I – Yield criteria and flow rules for porous ductile media. *Journal of Engineering Materials Technology*, ASME **99**, 2–15.

Hancock, J.W. (1982). Plasticity of porous metals. *Yield, Flow and Fracture of Polycrystals* (Edited by T.N. Baker), Applied Science Publishers, 151–183.

Hutchinson, J.W. (1973). Finite strain analysis of elastic-plastic solids and structures. *Numerical Solution of Nonlinear Structural Problems* ASME 17 (Edited by R.F. Hartung), New York.

Jagota, A., Hui, C.-Y. and Dawson, P.R. (1987). The determination of fracture toughness for a porous elastic-plastic solid. *International Journal of Fracture* **33**, 111–124.

Kim, M. and Pan, J. (1994). Effects of non-singular stresses on crack-tip fields for pressure-sensitive materials, Part 1: Plane strain case. *International Journal of Fracture* **68**, 1–34.

Li, F.Z. and Pan, J. (1990). Plane-strain crack-tip fields for pressure-sensitive dilatant materials. *Journal of Applied Mechanics* **57**, 40–49.

McMeeking, R.M. (1977). Finite deformation analysis of crack-tip opening in elastic-plastic materials and implications for fracture. *Journal of the Mechanics and Physics of Solids* **25**, 357–381.

Mesarovic, S. and Fleck, N.A. (1998). *Contact Between Elastic-Viscoplastic Particles* (Manuscript in preparation).

Miao, Y. and Drugan, W.J. (1993). Influence of porosity on plane strain tensile crack-tip stress fields in elastic-plastic materials: Part II. *Journal of Applied Mechanics* **60**, 883–889.

Miao, Y. and Drugan, W.J. (1995). Asymptotic analysis of growing crack stress/deformation fields in porous ductile metals and implications for stable crack growth. *International Journal of Fracture* **72**, 69–96.

Needleman, A. and Tvergaard, V. (1984). An analysis of ductile rupture in notched bars. *Journal of the Mechanics and Physics of Solids* **32**, 461–490.

Needleman, A. and Tvergaard, V. (1987). An analysis of ductile rupture modes at a crack tip. *Journal of the Mechanics and Physics of Solids* **35**, 151–183.

Needleman, A. and Tvergaard, V. (1987). An analysis of ductile rupture modes at a crack tip. *Journal of the Mechanics and Physics of Solids* **35**(2), 151–183.

Needleman, A. and Tvergaard, V. (1994). Mesh effects in the analysis of dynamic ductile crack growth. *Engineering Fracture Mechanics* **47**, 75–91.

Ogbonna, O. and Fleck, N.A. (1995). Compaction of an array of spherical particles. *Acta Metallurgica et Materialia* **43**(2), 603–620.

Rice, J.R. and Johnson, M.A. (1970). The role of large crack tip geometry changes in plane strain fracture. *Inelastic Behavior of Solids* (Edited by M.F. Kanninen, W.F. Adler, A.R. Rosenfield and R.I. Jaffee), McGraw-Hill, New York, 641–672.

Tvergaard, V. (1981). Influence of voids on shear band instabilities under plane strain conditions. *International Journal of Fracture* **17**, 389–407.

Tvergaard, V. (1982a). On localisation in ductile materials containing spherical voids. *International Journal of Fracture* **18**, 237–252.

Tvergaard, V. (1982b). Influence of void nucleation on ductile shear fracture at a free surface. *Journal of the Mechanics and Physics of Solids* **30**(6), 399–425.

Tvergaard, V. (1990). Material failure by void growth to coalescence. *Advances in Applied Mechanics* (Edited by J.W. Hutchinson and T.Y. Wu) **27**, 83–151.

Tvergaard, V. and Needleman, A. (1984). Analysis of the cup-cone fracture in a round tensile bar. *Acta Metallurgica* **32**, 157–169.

Tvergaard, V. and Hutchinson, J.W. (1992). The relation between crack growth resistance and fracture process parameters in elastic-plastic solids. *Journal of the Mechanics and Physics of Solids* **40**(6), 1377–1397.